

Article

# A biological-based photovoltaic electrochemical cell: modelling the impedance spectra

Eleonora Alfinito<sup>1\*</sup>, Francesco Milano<sup>2</sup>, Matteo Beccaria<sup>3</sup>, Rosella Cataldo<sup>4</sup>, Livia Giotta<sup>5</sup>, Massimo Trotta<sup>6</sup>, Maria Rachele Guascito<sup>7</sup>

<sup>1</sup>Department of Innovation Engineering, University of Salento, Via Arnesano, I-73100 Lecce, Italy; [eleonora.alfinito@unisalento.it](mailto:eleonora.alfinito@unisalento.it)

<sup>2</sup>CNR-ISPA Istituto di Scienze delle Produzioni Alimentari, Consiglio Nazionale delle Ricerche, Via Monteroni, Lecce, Italy; [francesco.milano@cnr.it](mailto:francesco.milano@cnr.it)

<sup>3</sup>Department of Mathematics and Physics "E. De Giorgi", University of Salento, Via Arnesano, I-73100 Lecce, Italy; [matteo.beccaria@unisalento.it](mailto:matteo.beccaria@unisalento.it)

<sup>4</sup>Department of Mathematics and Physics "E. De Giorgi", University of Salento, Via Arnesano, I-73100 Lecce, Italy; [rosella.cataldo@unisalento.it](mailto:rosella.cataldo@unisalento.it)

<sup>5</sup>Department of Biological and Environmental Sciences and Technologies (DiSTeBA), University of Salento, Via Arnesano, I-73100 Lecce, Italy; [livia.giotta@unisalento.it](mailto:livia.giotta@unisalento.it)

<sup>6</sup>CNR-IPCF Istituto per i Processi Chimico Fisici, Consiglio Nazionale delle Ricerche, Via Orabona 4, I-70125 Bari, Italy; [massimo.trotta@cnr.it](mailto:massimo.trotta@cnr.it)

<sup>7</sup>Department of Biological and Environmental Sciences and Technologies (DiSTeBA), University of Salento, Via Arnesano, I-73100 Lecce, Italy; [maria.rachele.guascito@unisalento.it](mailto:maria.rachele.guascito@unisalento.it)

\* Correspondence: [eleonora.alfinito@unisalento.it](mailto:eleonora.alfinito@unisalento.it); Tel.: +39-0832-297-766

**Abstract:** Bio-devices are designed to allow biological matter to perform *in vitro* almost the same functions it performs *in vivo*. Therefore, they can benefit from the specificities of such materials and are expected to perform better than traditional devices. On the other hand, the integration of biological material with electronic/electrochemical instrumentation requires careful attention and can produce unconventional results. In this paper, we describe the impedance response of an electrochemical cell that converts sunlight into electrical power. It uses the photosynthetic system known as Reaction Center, which is the core of photosynthesis in several living beings. Under illumination, an abrupt transformation drives the cell electrical response from insulator to conductor and a photocurrent is observed. The impedance spectrum shows a peculiar shape which significantly modifies with the protein activation. It has been analyzed by means of a graphical/analytical/numerical procedure. The modelling identifies an analogue electrical circuit, whose parameters give quantitative information about the underlying process. Finally, an appropriate normalization of data is proposed which validates data in dark and light and can be useful as a fast screening of measurements.

**Keywords:** impedance, photo-electrochemical cell, reaction centers

## 1. Introduction

The increasing demand for renewable energy, the necessity of reducing greenhouse gas emissions, and in general, the desirable evolution toward a more sustainable lifestyle have addressed the attention of researchers towards the development of innovative energy conversion devices, based on sun, wind, and thermal energy. Many commercial photovoltaic devices are available based on inorganic semiconductors. On the other side, there is a growing interest in mimicking sunlight energy conversion occurring in the natural photosynthetic process, such as in the Grätzel cell [1]. More recently, photoactive proteins extracted from plants, bacteria and archaea [2-5] have been tested

with the aim of producing biological-based photoelectrochemical cell (bPEC). In particular, much interest is devoted to the Reaction Center (RC) isolated from the purple photosynthetic bacterium *Rhodobacter sphaeroides*, thanks to its easy extraction and purification procedure, stability outside its natural environment, and large possibility of genetic manipulation for mutant construction [6]. In this kind of devices, RC retains *in vitro* the ability to drive a photocycle which is analogue to that performed *in vivo*, taking shape as a golden standard for third generation solar cells. Although the processes that the protein activates *in vivo* are known in enough detail, the features of the operating mechanisms in the electrochemical cell have to be clarified. Although the processes that the protein activates *in vivo* are known in sufficient detail, the features of the operating mechanisms in the electrochemical cell have to be clarified. In fact, many factors dramatically influence the behavior of the device, depending on the different kind of assembly, as for example, the protein location: dissolved in the bulk [5], or immobilized on the working electrode (WE) [7, 8, 9]; the type of employed mediators : endogenous or exogenous [10], the applied bias [11], and so on.

Electrochemical measurements, although simple to carry out, may be tricky to interpret because the processes occurring in the electrochemical cell (EC) are complex. They involve diffusion, multiple chemical equilibria, electron exchange between solid electrodes and dissolved species, and so on. Even more puzzling is the case of an EC in which an active layer deposited on the WE promotes, upon external stimulus, a displacement of the concentrations of electroactive species from their redox equilibria. This is the case of the analyzed bPECs in which the WE is functionalized with a photosynthetic protein that, upon light excitation, promotes processes resulting in photocurrent generation. The physico-chemical contents of the underlying processes require many different techniques to complete the picture of the various processes involved in the electrochemical cell. Results are of interest by both basic and applied research, due to possibility of improving the device response [11]. The information that can be extracted by classical chronoamperometric or voltammetric measurements can be complemented with those coming from Electrochemical Impedance Spectroscopy (EIS), a powerful technique in electrochemistry. It measures the cell properties by using a small perturbation, modulated in a wide range of frequencies, around the applied bias that can be, in turn, varied in a suitable range [12]. EIS is hence useful to explore the electric and dielectric response when the system is tested with small perturbation at equilibrium [12].

In the present paper, we outline a procedure to interpret the impedance response of a bPEC, synergistically using graphical, analytical and numerical investigations. The proposed theoretical modelling is tested against two independent datasets that, after a normalization procedure, result in agreement with each other, ensuring that, in the explored bias range, the physico-chemical mechanisms of the process do not change, i.e. the device, particularly the protein substrate, is not altered during the measurement time.

## 2. Experiments

Reaction Centers were extracted and purified from the bacterium *Rhodobacter Sphaeroides* as previously described [13], obtaining a 30  $\mu\text{M}$  stock solution in Tris 20 mM, EDTA 1 mM, LDAO 0.03% pH 8.0, stored at  $-20\text{ }^{\circ}\text{C}$ .

The bPEC is a three electrode EC made of screen printed electrodes (SPEs) DRP-550 (DropSens, Spain) with a Pt round-shaped WE of  $0.12\text{ cm}^2$  surrounded by a Pt counter electrode (CE) and an Ag quasi-reference electrode (RE) whose potential has been estimated to be +210 mV vs NHE. The aqueous medium used for electrochemical measurements was potassium phosphate 90 mM, TX 0.03% v/v, pH 7.0,  $I = 0.2$  (PB90T). The potentiostat was an Ivium Vertex One controlled by computer with the IviumSoft program. Modified SPEs were obtained by depositing PVA/RC films onto the Pt WE surface using two different procedures. In the first case, 9  $\mu\text{L}$  of the RC stock solution were deposited and dried onto the WE and subsequently 9  $\mu\text{L}$  of PVA 0.5% has been added and dried. In the second case a mixture of 9  $\mu\text{L}$  RC stock + 1  $\mu\text{L}$  PVA 5% has been prepared; 3  $\mu\text{L}$  of this solution were deposited and dried onto the WE; then a second aliquot of 3  $\mu\text{L}$  has been added and dried. In both cases the electron donor ferrocenemethanol (FcnMeOH) and the electron acceptor

decylubiquinone (dQ) have been added in the solution to a final concentration of 300  $\mu\text{M}$  and 100  $\mu\text{M}$  respectively, to drive the RC photocycle [14]. The bPEC response has been recorded in dark and under light exposure using a light emitting diode (LED) centred at 800 nm with full width at half maximum of 30 nm, providing a light intensity of 25  $\text{mW}/\text{cm}^2$  at the surface of the WE. EIS measurements were performed at controlled WE potential of 0.0, -25, -50, -75 and -100 mV vs the Ag quasi-RE with a modulation of 10 mV and frequency range 1–100 KHz for the first electrode and 0.1–100 KHz for the second electrode. The largest light-dark difference in response is obtained at 0.0 mV applied bias, which corresponds to the measured open circuit potential (OCP) in the dark. Data were collected in two different functionalization conditions of the WE, and produce qualitatively similar impedance responses, although quantitatively different. Figures 1-4 report the datasets 1&2 in the Nyquist and Phase representation (symbols). The Nyquist plot is the drawing of the imaginary vs. the real part of impedance, and the Phase plot, is the drawing of the impedance phase angle vs. the frequency. Lines come from the modelling.

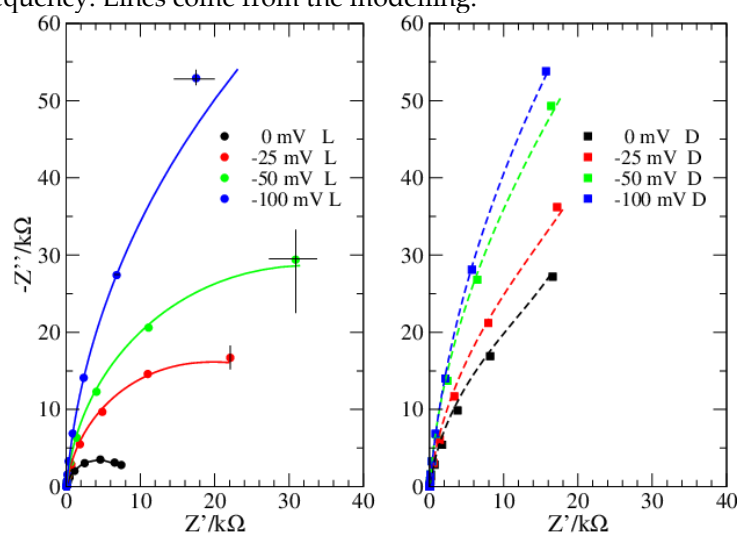


**Figure 1.** Dataset 1. Data taken in light (circles) and dark (squares). Lines reproduce data from simulations.

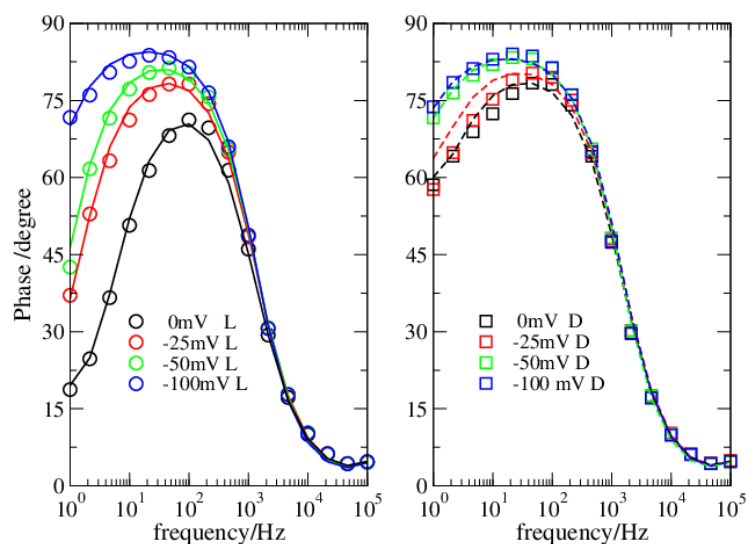


**Figure 2.** Dataset 1. Data in light (circles) and dark (squares). Lines reproduce data from simulations.

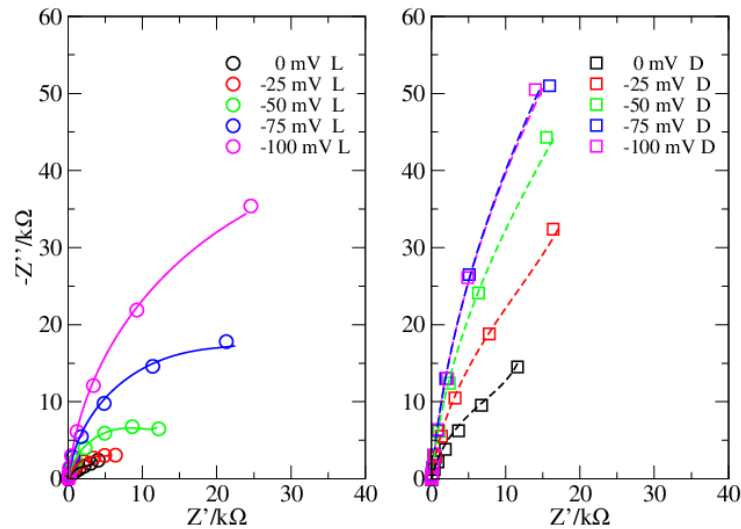


**Figure 3.** Dataset 2. Data in light (circles) and dark (squares). Lines reproduce data from simulations.

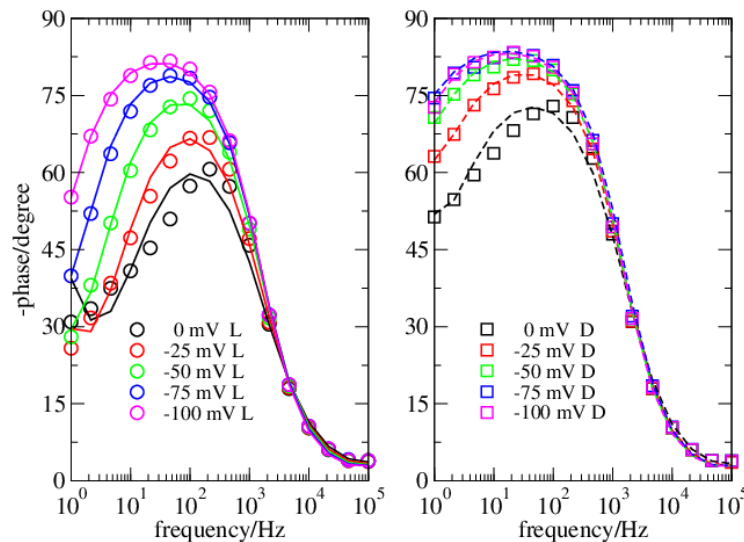


**Figure 4.** Dataset 2. Data in dark (squares) and light (circles). Lines reproduce data from simulations.

### 3. Theory

The strategy we follow is based on the design of an equivalent electrical circuit (EEC) [15-17], which maps the electronic response into a minimal set of circuit elements. It successfully applies when the different characteristic times of each element have negligible overlaps. Although EEC is a very simplified description of the actual phenomena, it is quite powerful in data interpretation. The procedure develops in two steps, the first one, qualitative, is based on the graphical analysis of the impedance spectrum. It allows to identify the main elements of the EEC, associating them with different frequency ranges [15, 17]. Once the EEC has been designed, the quantitative step is taken, calculating the best-fitting value of the circuit elements. Finally, the main phenomena inside the electrochemical cell are pulled off these values. Analyses performed under different bias and illumination conditions help to produce a complete model of the physico-chemical mechanism underlying the impedance response.

#### 2.1 Graphical analysis

As widely shown in the literature [15], in the simplest cases the graphical features of the Nyquist and Phase plots may suggest a good estimate of the EEC parameters [15, 17].

In the present investigation, the Nyquist plots appear different when obtained in dark or in light (Figures 1, 3), thus suggesting a different modelling for the two conditions. Instead, the Phase plots ensure this is not the case (Figures 2, 4). Specifically, in light, the Nyquist plots are arcs while in dark they tend to a linear shape. On the other side, the Phase plots have a very similar shape both in dark and light, the major differences are at the OCV, and reduce considerably at more negative bias. The analyzed Phase plots appear like bell-shaped curves, which suggest a Voigt element as the main term [17]. The maximum of the curve, which roughly determines the Voigt characteristic time, is in the middle of the intermediate frequency range of the bPEC. At high frequencies the phase angle reaches the frequency axis, thus revealing a solution impedance element. Finally, at low frequencies, the curve shows a puzzling shape that strongly depends both on the applied bias and on the illumination conditions. Specifically, it remains far from zero and its absolute value becomes larger by increasing the bias. In light, this deviation from the ideal case is milder. This behavior has been attributed to a capacitor [17], which pushes the phase angle toward  $90^\circ$ .

## 2.2 The EEC

The suitable EEC is displayed in Figure 5 and contains a quite standard arrangement, made of three elements: a solution impedance  $Z_s$  and a Voigt circuit, both in series with a capacitor,  $C_{DL}$ . This latter term is the most distinctive one of this EEC and takes into account the differences between dark and light: if small (dark), it produces quite a linear Nyquist plot, otherwise, when large (light), it allows the semicircular shape to emerge. In Figure 5, the Nyquist plot of the EEC is drawn for decreasing values of  $C_{DL}$ , from  $C_{DL}=C$  to  $C_{DL}=0.001 C$ , with  $C$  being the capacitor of the Voigt element.

Each of the three EEC elements is associated with a specific conduction term, relevant in a specific frequency range. In the high frequency (HF) range, the response is dominated by the solution parameters, i.e. the impedance ( $Z_s$ ), in which the resistance  $R_s$  is in parallel with the capacitor  $C_s$ . It mimics the charge transport and the polarization inside the solution, mainly due to the supporting electrolytes. However, in the present case, the resistance alone is used to describe this impedance contribution. However, in the present case, the polarization is detectable, although tiny. Since both  $R_s$  and  $C_s$  are small, the impedance characteristic time is also small and corresponds to a high characteristic frequency. In the intermediate frequencies, the Voigt element describes the electronic conduction inside the electrode and the ability of the redox couple to drain electrons. Electrons are transferred between the redox couple dissolved in solution and the electrode made of a Pt-PVA-RC inhomogeneous substrate. The electrode conductive properties are not completely understood and are expected to change in light. As a matter of fact, while Pt and PVA are poorly affected by visible light, under illumination RC promotes an electron flow from  $FcnMeOH$  to  $dQ$ , altering the redox equilibria of these dissolved species. In the applied bias conditions electrons eventually flow towards the oxidized species  $FcnMeOH^+$  generated by the photoexcitation of RC, i. e. the conduction at the interface electrode/solution varies with the amount of  $FcnMeOH^+$ . Current does not depend linearly on the applied bias, but it is governed by Nernst's law [12]. In other words, making the bias more negative, the amount of  $FcnMeOH^+$  reduces and  $R_{CT}$  grows, therefore the current tends to an asymptotic value, which depends on the initial concentration of  $FcnMeOH$ . Despite being so complex, this sequence of events happens in cascade and a single resistance  $R_{CT}$  may be a sufficient description.

To account for the dielectric aspects, the capacitor  $C$  is put in parallel with  $R_{CT}$ . In most cases, as in the present analysis, deviations from the ideal response are detected and therefore the circuit element describing the polarization is mapped into a constant phase element  $Z_{CPE}$ . Mathematically, it is obtained by introducing a phase,  $\alpha$ , in the standard capacitor impedance:

$$Z_{CPE} = \frac{r}{(j\omega\tau)^\alpha} = r \frac{\cos(\pi\alpha/2) - j\sin(\pi\alpha/2)}{(\omega\tau)^\alpha} \quad (1)$$

where  $r$  is the  $Z_{CPE}$  resistance, here  $R_{CT}$ ,  $\tau$  the characteristic time, and  $\tau/r$  is the associated capacitor,  $C$ .

Basically, a Voigt element made of a  $Z_{CPE}$  instead of a simple capacitor, distributes part of the impedance in the dissipative term, so reducing the reactance. In other terms, it describes a system more entropic than the ideal one, i. e.  $\alpha = 1$ . Sometimes,  $\alpha < 1$  is used to describe a condition in which many characteristic times are present: when they are very close, they can interfere, so enhancing the entropic part. A typical case is represented by a sample with a significant porosity, in which each pore contributes to the impedance with a different time [12]. The corresponding Nyquist plot deviates from ideal semicircle, showing a flattening.

Finally, the capacitive impedance,  $Z_{CDL} = r/j\omega\sigma = 1/j\omega C_{DL}$  also accounts for the redox couple. Specifically, in dark, the amount of  $FcnMeOH$  around the WE is so high that it reduces the electronic conduction, allowing only a small leakage current. In light, the leakage current increases. The elementary capacitor  $C_{DL}$ , when interpreted as a parallel plate element, enables a simple picture of the phenomenon:  $FcnMeOH$  forms a layer of size  $L$  around the WE and the larger  $L$  the smaller  $C_{DL}$ . In dark and for more negative bias values,  $L$  grows and  $C_{DL}$  decreases. This element adds a pure imaginary term to the total impedance, becoming even more relevant at decreasing frequencies,  $f < 1/2\pi\sigma$  (see Figure 5).

### 2.3 The custom-fit software

The optimal value of the EEC parameters has been determined by a custom Python code that minimizes a suitable  $\chi^2$  function, measuring the deviation from the experimental complex-valued impedance. In particular, we exploited the *least squares* function in the *optimize* module of the Python-based open-source *SciPy* library [13]. We remark that the EEC parameters appear in the theoretical expression of the complex impedance in a non-linear way.

The values of the circuit elements are reported in Tables 1 & 2 for datasets 1 & 2, respectively.

Dataset 1 shows values of  $R_{CT}$  and  $C$  larger than dataset 2, in each experimental condition. The value of the solution impedance is practically the same for both datasets. The “roughness” parameter,  $\alpha$ , appears smaller for the dataset 2, mainly at the OCV. This suggests that the samples used for dataset 2 were more porous than samples of dataset 1. Making the bias more negative,  $\alpha$  tends to 1 for both datasets, i.e. the role of the specific substrate becomes less relevant. In both cases, at growing values of the applied bias, the impedance responses in light becomes even more similar to that measured in dark. The EEC values for each dataset are reported in Tables 1&2.

Bias (mV)	$R_{CT}$ ( $\Omega$ )	$\alpha$	$C$ ( $\mu F$ )	$C_{DL}$ ( $\mu F$ )	$\varepsilon$
0 L	7860	0.89	3.3	110	0.89
0 D	28000	0.89	4.6	10	1.76
-25 L	30677	0.92	3.2	43	1
-25 D	38900	0.90	4.6	82	2.12
-50 L	53000	0.94	3.0	40	1.06
-50 D	60000	0.93	4.5	6.1	2.49
-100 L	96000	0.94	3.6	10	1.63
-100 D	105000	0.94	4.4	7.2	2.11

**Table 1.** EEC parameters for Dataset 1. Nominal impedance solution is less than 63  $\Omega$ .

Bias	$R_{CT}$	$\alpha$	$C$	$C_{DL}$	$\varepsilon$
------	----------	----------	-----	----------	---------------

(mV)	( $\Omega$ )	( $\mu\text{F}$ )	( $\mu\text{F}$ )	( $\mu\text{F}$ )	( $\mu\text{F}$ )
0 L	4000	0.76	6.25	100	0.8
0 D	15700	0.85	5.3	18	1.37
-25 L	6521	0.83	4.6	83	0.87
-25 D	27000	0.89	5.4	8.8	1.95
-50 L	13300	0.89	3.6	56	1.0
-50 D	50543	0.91	5.0	6.7	2.35
-75 L	29458	0.92	3.3	31	1.1
-75 D	81750	0.915	5.1	6.6	2.42
-100 L	59000	0.93	3.3	19	1.25
-100 D	87000	0.92	4.9	6.9	2.29

**Table 2.** EEC parameters for Dataset 2. Nominal impedance solution is less than 60  $\Omega$ .

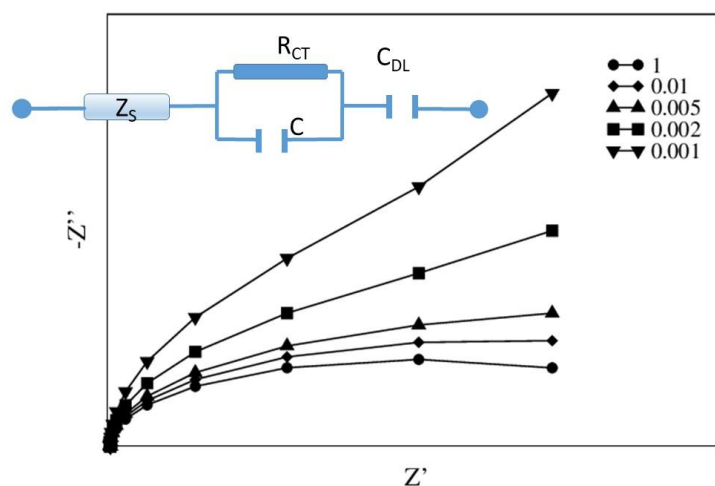


**Figure 5.** The proposed EEC and the expected Nyquist plot for  $C_{DL}=C, 0.01C, 0.005C, 0.002C, 0.001C$ .

#### 2.4 Analytical vs. computational procedure.

Tables 1 & 2 summarize the results of the data analysis performed with a best-fitting software. Nevertheless, as we have highlighted in a previous paper [11], even the best software needs an analytical control. This is particularly true when the number of parameters is high, the experimental errors are relevant, and, in general, the system is so complex that several solutions are allowed. Multiple possible choices of the fitting parameter give apparently similar results, often with comparable confidence levels. A visual inspection of Nyquist and Phase plot can help in selecting the best one, but it is not sufficient. In general, this is due to the very wide frequency range, so different least-square solutions can be found by privileging different frequency ranges.

A tool that is always helpful to test the quality of results, is the comparison with a benchmark. In more simple cases, when a single Voigt element is sufficient to describe the data [14] a normalization procedure is adopted to standardise the device response. The normalization factor is the impedance evaluated at the frequency  $f=1/(2\pi\tau)$ , then the normalized variables are:  $x = 2Z'(\omega\tau)/Z'(1)$ ,  $y = 2Z''(\omega\tau)/Z''(1)$ , being  $Z'(1) = -Z''(1) = \frac{1}{2}R_{CT}$ . In such a way, the curves obtained with different values of the Voigt parameters collapse into a single arc of radius  $\frac{1}{2}$ .

In the present case, neglecting the HF impedance, the impedance is described by [17]:

$$\text{Re}Z \equiv Z'(\omega\tau) = \frac{R_{CT}[1 + (\omega\tau)^\alpha \cos(\pi\alpha/2)]}{[1 + (\omega\tau)^{2\alpha} + 2(\omega\tau)^\alpha \cos(\pi\alpha/2)]}, \quad (2a)$$

$$\text{Im}Z \equiv Z''(\omega\tau) = -\frac{R_{CT}(\omega\tau)^\alpha \sin(\pi\alpha/2)}{[1 + (\omega\tau)^{2\alpha} + 2(\omega\tau)^\alpha \cos(\pi\alpha/2)]} - \frac{1}{\omega C_{DL}}. \quad (2b)$$

Therefore, for  $f=1/(2\pi\tau)$ , the real and imaginary parts are different and read:

$$Z'(1) = \frac{1}{2}R_{CT}, \quad Z''(1) = -\frac{1}{2}\left(\frac{\sin(\pi\alpha/2)}{[1 + \cos(\pi\alpha/2)]} + \frac{2\tau}{C_{DL}R_{CT}}\right)R_{CT} \equiv -\frac{1}{2}\varepsilon R_{CT}. \quad (3)$$

The enhancement factor  $\varepsilon$  (see Table 1 &2) is close to 1 in light and close to 2 in dark and grows when the applied bias becomes more negative. For  $\varepsilon=1$ , the single Voigt circuit response is reproduced (ideal condition), while values less than 1 give a flattened Voigt circuit (with a  $Z_{CPE}$  element). It is worthy of note that the ideal condition is achieved as the combination of two competitive effects: a suppression due to the electrode roughness ( $\alpha$ ) which increases the dissipative term ( $R_{CT}$ ) compared to the energy storage term and the enhancement due to the capacitor  $C_{DL}$ , which restores the energy storage. On the other side, when the storage term overcomes the dissipative term, electron transport is inhibited. The normalized Nyquist plots for both datasets are now obtained by using Equation 3 and are reported in Figures 6 &7.

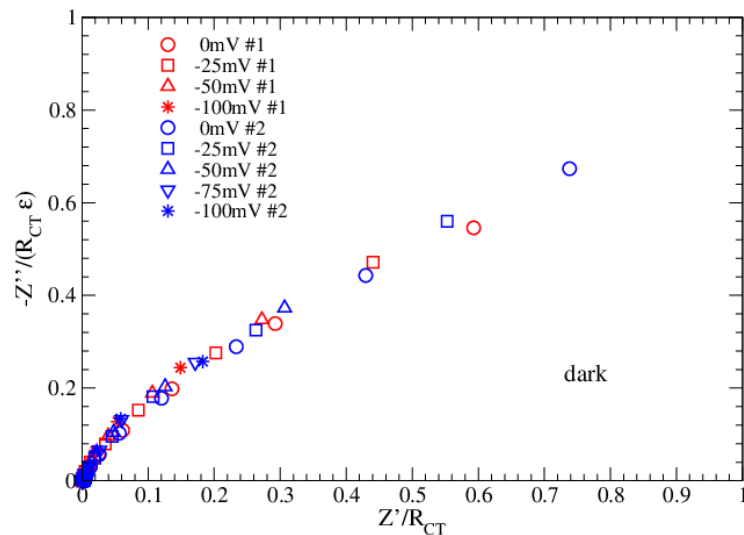


**Figure 6.** Normalized Nyquist plots in dark for dataset 1 and 2.

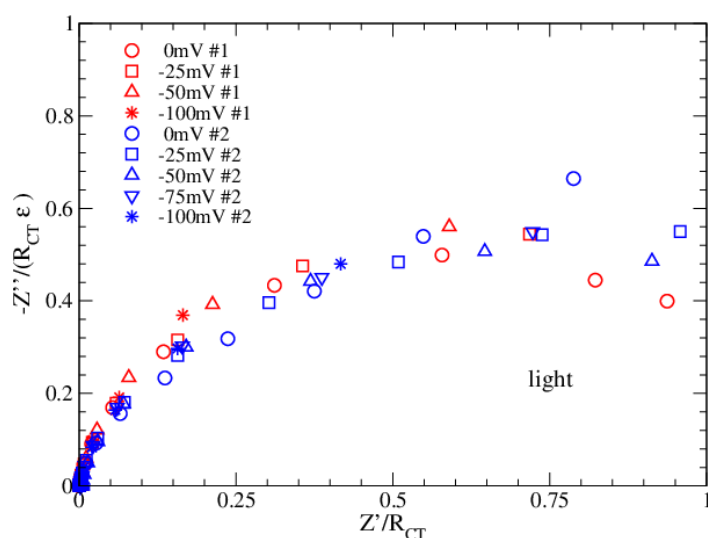


**Figure 7.** Normalized Nyquist plots in light for dataset 1 and 2.

Figures 6&7 confirm that the proposed EEC correctly describes the impedance of the bPEC, in each possible condition of bias and functionalization. The  $\varepsilon$  parameter, entering the normalization of the vertical axis, plays an important role in the universal data collapse. From this perspective, it can be used to discriminate among different fitting solutions. Furthermore, comparing the results in dark and light, it emerges that measurements in light are more critical at low frequencies (1-2 points), and this is probably due to a thermal effect related to the long-time exposure.

## Conclusions

In this paper, we have discussed the impedance spectroscopy data of a bio-based photovoltaic device, using a graphical/analytical/numerical procedure. The device is very sensitive to light and gives the best performances in the absence of applied potential. The modelling is performed by means of a non-standard equivalent electrical circuit, simulated by using an open-source code. Here we apply this technique to two series of measurements, both performed in light and dark, using different bias values. The datasets refer to quite different functionalizations of the working electrode. A suitable normalization procedure is introduced that shows that both datasets reflect the same phenomenon, with illumination promoting the system from insulator to conductor. The key element in the equivalent electrical circuit to signal the insulator/conductor transition is a capacitor,  $C_{DL}$ , which is related to the concentration of the oxidized specie of the redox couple. The described modelling is rather simple to implement and the normalization procedure that we proposed confirms our interpretation and can be used to standardize data and identify errors in measurements.

**Acknowledgments:** This research was supported in part by the Italian Ministry of Education, University and Research (MIUR) with the grant Project FFABR 2017.

**Author Contributions:** E.A. conceived and designed theory; F.M., L.G. and M.R.G conceived and performed measurements; M.B. conceived and designed the software; all authors wrote the paper.

**Conflicts of Interest:** The authors declare no conflict of interest.

## References

1. O'Regan, B.; Grätzel, M. A low-cost, high-efficiency solar cell based on dye-sensitized colloidal TiO<sub>2</sub> films. *Nature* **1991**, *353* (6346), 737.
2. Alfinito, E.; Pousset, J.; Reggiani, L.; Lee, K. Photoreceptors for a light biotransducer: a comparative study of the electrical responses of two (type-1) opsins, *Nanotechnology* **2013**, *24*(39), 395501.

3. Alfinito, E; Reggiani, L. Mechanisms responsible for the photocurrent in bacteriorhodopsin. *Phys. Rev. E* **2015**, *91*(3), 032702.
4. Białek, R.; Swainsbury, D. J.; Wiesner, M.; Jones, M. R.; Gibasiewicz, K. Modelling of the cathodic and anodic photocurrents from *Rhodobacter sphaeroides* reaction centres immobilized on titanium dioxide. *Photosynthesis research* **2018**, *138*(1), 103-114.
5. Milano, F.; Ciriaco, F.; Trotta, M.; Chirizzi, D.; De Leo, V.; Agostiano, A.; Valli, L.; Giotta, L.; Guascito, M.R. Design and modelling of a photo-electrochemical transduction system based on solubilized photosynthetic reaction centres. *Electrochimica Acta* **2019**, *293*, 105-115.
6. Espiritu, E.; Chamberlain, K. D.; Williams, J. C.; Allen, J. P. Bound manganese oxides capable of reducing the bacteriochlorophyll dimer of modified reaction centers from *Rhodobacter sphaeroides*. *Photosynthesis Research* **2019**, *143*(2), 129-141. DOI: 10.1007/s11120-019-00680-3.
7. Chatzipetrou, M.; Milano, F.; Giotta, L.; Chirizzi, D.; Trotta, M.; Massaouti, M.; Guascito, M.R.; Zergioti, I. Functionalization of gold screen printed electrodes with bacterial photosynthetic reaction centers by laser printing technology for mediatorless herbicide biosensing. *Electrochemistry Communications* **2016**, *64*, 46-50, <https://doi.org/10.1016/j.elecom.2016.01.008>.
8. Ravi, S.K.; Tan, S. C. Progress and perspectives in exploiting photosynthetic biomolecules for solar energy harnessing. *Energy Environ. Sci.* **2015**, *8*, 2551-2573.
9. Kamran, M.; Delgado, J.D.; Friebe, V.; Aartsma, T.J.; Frese, R.N. Photosynthetic protein complexes as bio-photovoltaic building blocks retaining a high internal quantum efficiency. *Biomacromolecules* **2014**, *15*, 2833-2838.
10. Friebe, V.M.; Millo, D.; Swainsbury, D.J.K.; Jones, M.R.; Frese, R.N. Cytochrome c provides an electron-funneling antenna for efficient photocurrent generation in a reaction center biophotocathode. *ACS Appl. Mater. Interfaces* **2017**, *9*, 23379-23388.
11. Guascito, R.; et al. Physico-chemical characterization of a novel protein-based electrochemical solar cell, in preparation.
12. Bard, A.J.; Faulkner, L. *Electrochemical Methods: Fundamentals and Applications*. 2nd ed; John Wiley & Sons: New York, 2000.
13. De Leo, V.; Catucci, L.; Falqui, A.; Marotta, R.; Striccoli, M.; Agostiano, A.; Comparelli, R.; Milano, F. Hybrid Assemblies of Fluorescent Nanocrystals and Membrane Proteins in Liposomes. *Langmuir* **2014**, *30*(6), 1599-608.
14. Milano, F.; Gerencsér, L.; Agostiano, A.; Nagy, L.; Trotta, M.; Maróti, P. Mechanism of Quinol Oxidation by Ferricenium Produced by Light Excitation in Reaction Centers of Photosynthetic Bacteria. *J. Phys. Chem. B* **2007**, *111*(16), 4261-4270.
15. Orazem, M.E.; Tribollet, B. *Electrochemical impedance spectroscopy*. Vol48; Publisher: John Wiley & Sons, 2011.
16. Sacco, A. Electrochemical impedance spectroscopy: Fundamentals and application in dye-sensitized solar cells. *Renewable and Sustainable Energy Reviews* **2017**, *79*, 814-829.
17. Guascito, M. R.; Alfinito, E.; Cataldo, R.; Giotta, L. Tips for a (simple) interpretation of the impedance response of an electrochemical cell. *IEEE Sens. J.* **2019**, *19*(23), 11318-11322.
18. Huang, J. Diffusion impedance of electroactive materials, electrolytic solutions and porous electrodes: Warburg impedance and beyond. *Electrochim. Acta* **2018**, *281*, 170-188.
19. SciPy.org. Available online: <https://scipy.org> (SciPy 1.2. released 2020-01-21).
20. Alfinito, E.; Pousset, J.; Reggiani, L. *Proteotronics: Development of Protein-Based Electronics*. Pan Stanford Publishing: Danvers (USA), 2015; ISBN 978-981-4613-63-7.